

On-line Inertia Identification Algorithm for PI Parameters Optimization in Speed Loop

Li Niu, Dianguo Xu, *Senior Member, IEEE*, Ming Yang, Xianguo Gui, and Zijian Liu

Abstract—This paper presents a novel on-line inertia identification method with a load torque observer to optimize the speed loop PID parameters of a servo system. The proposed inertia identification algorithm in this paper adopts the fixed-order recursive empirical frequency-domain optimal parameter estimation to improve the speed loop performance. A load torque observer is employed in order to obtain a more precise value of inertia. Then, the method of speed loop PI parameters optimization with the identified inertia and load torque is deduced in frequency domain. Compared with the recursive least square algorithm, the effectiveness of the proposed method is demonstrated by the simulation and experimental results.

Index Terms—Load torque observer, on-line inertia identification, PID optimization, speed loop control.

I. INTRODUCTION

SERVO pack, as an important actuator in the automation control system, has been widely used in civilian and industrial fields, due to its characteristic of high precision, high power density, and high reliability. The utilization of servo pack can save cost, raise productivity, and even protect workers from some specific hazardous environment. Therefore, a lot of literatures have been published to improve the performance of servo pack [1]–[3]. As the performance of current (torque) loop, which is the inner loop of servo systems, is the most critical for the performance of a servo system, the researchers have proposed various control strategies to improve the current-loop performance. The strategies include celebrated field oriented control [4]–[7], which makes it possible for ac motors to be controlled in a similar way as the dc motors. Another strategy, the direct torque control (DTC) can improve the dynamic performance of ac motors [8], [9]. The best linear control strategy for ac motors is the predictive control, which is based on the dead-beat control theory [10]–[14]. Moreno *et al.* [15], and Huerta *et al.* [16] proposed a modified predictive current control method based

on Luenberger observer, that gives additional gain margin and phase margin for the control system in order to effectively improve the stability of the control system. The modified predictive current control method is adopted in this paper to obtain an optimal performance of the current loop.

Then, the performance of speed loop would be the main research target after the current loop performance becomes optimal. Due to the complex working environment of the servo system, the moment of inertia is changing all the time. So the knowledge of inertia is a critical factor for speed loop performance. Researchers have proposed various methods for motor inertia identification, which can be summarized into two categories: off-line inertia identification [17], [18] and on-line inertia identification [19]–[24].

Lee *et al.* [17] and Choi *et al.* [18] proposed an inertia identification method using the information of torque and position. But the identification method needs a specific speed command, and the method can only estimate the moment of inertia off-line.

In [19], a full-order Luenberger observer is reconstructed to estimate the inertia information. And the full-order Luenberger observer is also adopted in [20], where the inertia is estimated by observing the position error and the estimated inertia is one of the parameters in the identification algorithm. Thus, the full-order observer will be severely affected by the initial value of the moment of inertia, and in the worst case, the system will be unstable. Lin *et al.* [21] utilized a reduced-order Luenberger observer to estimate the load torque, and then, uses the estimated load torque to correct the inertia information. It is similar in [19] and [20] that there is still an estimated error of the Luenberger observer whether the inertia information is accurate or not. Okamura *et al.* [22] and Andoh [23] used a recursive least square (RLS) method or recursive extended least square to estimate the inertia information. But the estimated result of RLS has some oscillation on the speed change, and the estimated error of RLS is large at low speed. Andoh [24] calculates directly the inertia value with the equation of motion, however, the estimated result is more susceptible to the sampling error. In conclusion, there has not been any identification algorithm that is of high precision and robustness against system delay and error.

In this paper, a novel inertia identification algorithm is proposed. Based on the original empirical frequency-domain optimal parameter estimation, the proposed fixed-order empirical frequency-domain optimal parameter estimation (FOREFOP) reduces the matrices dimensions of intermediate matrix and alleviates the computing burden on the processor [25], [26]. The estimated result of the FOREFOP algorithm is more precise, and more robust against system delay and sampling errors. In order to overcome the disturbance of load torque, a load torque

Manuscript received July 30, 2013; revised October 8, 2013 and December 10, 2013; accepted February 11, 2014. Date of publication February 20, 2014; date of current version October 7, 2014. This work was supported in part by the National Natural Science Foundation of China 61273147 and the Power Electronics Science and Education Development Program of Delta Environmental & Educational Foundation. Recommended for publication by Associate Editor R. Kennel.

The authors are with the School of Electrical Engineering and Automation, Harbin Institute of Technology, Harbin 150001, China (e-mail: nli9698@gmail.com; xudiang@hit.edu.cn; yangming@hit.edu.cn; xianggui@hit.edu.cn; 992513833@qq.com).

Color versions of one or more of the figures in this paper are available online at <http://ieeexplore.ieee.org>.

Digital Object Identifier 10.1109/TPEL.2014.2307061

observer based on Gopinath's method is also adopted [27]. Natori *et al.* [28] and Kobayashi *et al.* [29] have proved that the Gopinath load torque observer is an effective way to obtain the knowledge of load torque. As the PI controller is the most popular regulator for the speed loop [30], [31], the calculation of optimal PI parameters in frequency domain is given. Simulation and experiment results show that, compared with the RLS algorithm, the proposed FOREFOP algorithm is more stable and can suppress the sampling delay and sampling errors. In addition, the proposed control structure will guarantee the speed loop control performance in real time.

This paper is organized as follows. First, the structure of speed control loop is given in Section II. Then, Section III presents the load torque observer adopted in this paper and the selection of observer coefficient is discussed. In Section IV, the proposed FOREFOP estimation is introduced, and the simulation comparison with RLS is also given. Then, the calculation of PI parameters in frequency domain is shown in Section V. The experiment results are demonstrated in Section VI. At last, Section VII summarizes this paper.

II. STRUCTURE OF THE SPEED LOOP

In general, a servo system operates in the position loop. However, the control performance of the speed loop, as the inner loop of position loop, is an important factor for the position loop control performance. In this section, we illustrate the traditional speed loop control structure with PID regulator for servo systems.

The equation of motion of a PMSM can be expressed as

$$\frac{d\omega}{dt} = -\frac{B}{J}\omega - \frac{1}{J}\tau_L + \frac{1}{J}T_e \quad (1)$$

where J is the moment of inertia of the servo motor, B is the friction coefficient, ω is the rotor angular velocity, τ_L is the load torque, and T_e is the electromagnet torque of the motor.

For most applications, the load torque τ_L is a slow time-varying variable, and its differential can be shown as follows:

$$\frac{d\tau_L}{dt} = 0. \quad (2)$$

The traditional method for speed loop control is to use a PID regulator as speed controller. But in most cases, the PID regulator will become a PI regulator because sometimes the effect of differential can introduce a large oscillation into the speed loop. The transfer function of PI regulator $G_{PI}(s)$ can be expressed as

$$G_{PI}(s) = K_P + \frac{K_I}{s} \quad (3)$$

where K_P is the proportional coefficient, K_I is the integral coefficient, and s is the differential operator.

Then, the close-loop diagram of speed loop with PI regulator is shown in Fig. 1, where the current controller adopts the predictive current control algorithm in order to realize the optimal current control performance.

In most applications of servo motors, the load inertia and load torque vary frequently. Hence, the high-performance servo

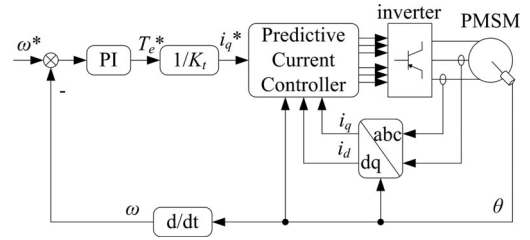


Fig. 1. Structure of speed loop with PI regulator.

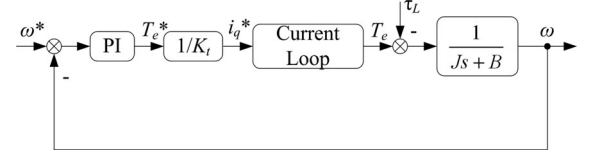


Fig. 2. Simplified diagram of speed control loop.

systems have to observe both the load inertia and load torque, and must adjust the PI parameters on-line according to the rotor inertia. A simplified speed loop diagram is shown in Fig. 2 for the convenience of analysis.

III. LOAD TORQUE OBSERVER

A. Model of Load Torque Observer

The mathematical model of motor speed loop (4) is obtained by (1) and (2). The load torque acts as a disturbance in the speed loop and it cannot be measured directly. Therefore, we need to find a method to observe load torque by the variables that can be measured like the motor current and speed

$$\begin{bmatrix} \frac{d\omega}{dt} \\ \frac{d\tau_L}{dt} \end{bmatrix} = \begin{bmatrix} -\frac{B}{J} & -\frac{1}{J} \\ 0 & 0 \end{bmatrix} \begin{bmatrix} \omega \\ \tau_L \end{bmatrix} + \begin{bmatrix} \frac{1}{J} \\ 0 \end{bmatrix} T_e. \quad (4)$$

Various types of load torque observers have been used in the speed control system, and among them the Gopinath method is an effective way to construct the load torque observer. Then, we construct the load torque observer as

$$\frac{d\tilde{\tau}_L}{dt} = \frac{l}{J}\tilde{\tau}_L + \left(\frac{lB}{J} + \frac{l^2}{J}\right)\omega - \frac{l}{J}T_e \quad (5)$$

$$\hat{\tau}_L = \tilde{\tau}_L + l\omega \quad (6)$$

where l is the observer coefficient, $\tilde{\tau}_L$ is the intermediate variable of the load torque observer, and $\hat{\tau}_L$ is the estimation of load torque.

The estimation equation in frequency domain of the load torque observer (7) can be obtained from (5) and (6), and the diagram of the proposed load torque observer is shown in Fig. 3

$$\hat{\tau}_L = \frac{(B + Js)l\omega - lT_e}{Js - l}. \quad (7)$$

B. Value Range of Coefficient in Load Torque Observer

Based on Gopinath's theory, the estimated load torque $\hat{\tau}_L$ will converge to the actual value as fast as $e^{(l/J)t}$. That means

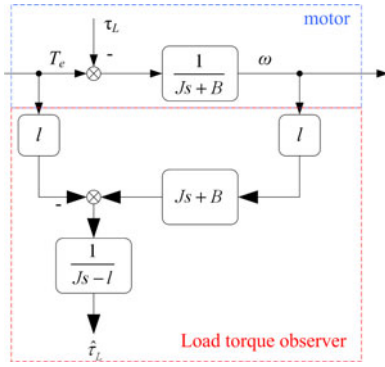


Fig. 3. Diagram of the proposed load torque observer.

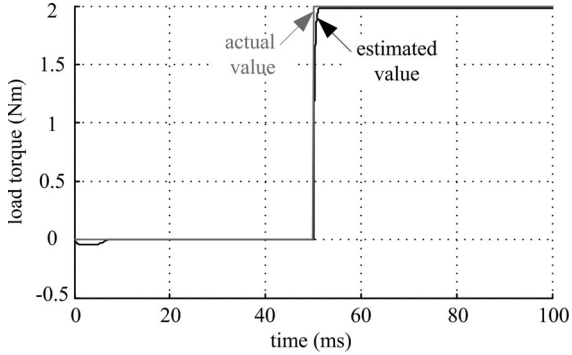


Fig. 4. Simulation of load torque observer in continuous-time domain.

the convergent speed l/J should less than 0, i.e., the observer coefficient $l < 0$. The simulation waveform of load torque observer is shown in Fig. 4, where the speed command steps from 0 to 1000 r/min at 0 s, the load torque steps from 0 to 2 N•m at 0.05 s, and $l = -1$. The simulation waveform shows that the proposed load torque observer has excellent performance of tracking the variation of the actual load torque, and the estimation error is within 0.85% in steady state.

The only constraint for l in continuous-time domain is $l < 0$, however, the constraint for l is more rigid in the discrete-time domain. Therefore, we should study on the effect caused by the discretization of the proposed observer as digital controllers are used in almost all modern servo systems.

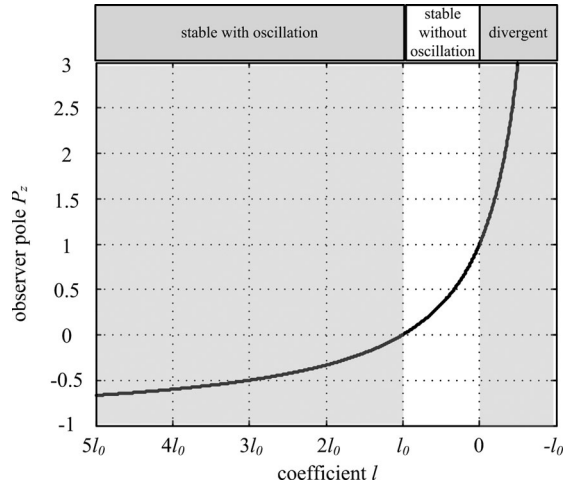
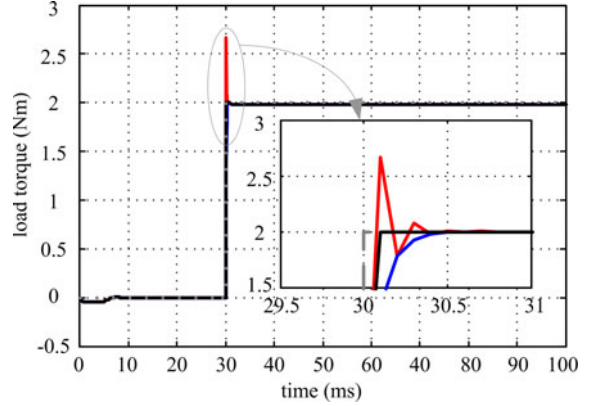
By applying the bilinear transformation $s = 2(1-z^{-1})/[T(1+z^{-1})]$, (7) can be rewritten in (8). And the pole of the characteristic equation is expressed as (9), where T is the sampling period

$$\hat{\tau}_L = \frac{(BT + 2J)l\omega - lTT_e + z^{-1}[(BT - 2J)l\omega - lTT_e]}{2J - lT - z^{-1}(2J + lT)} \quad (8)$$

$$P_z = \frac{2J + lT}{2J - lT}. \quad (9)$$

In order to avoid the oscillation of the estimated result, the pole of the discrete load torque observer P_z should be in the interval $(0, 1)$, i.e.

$$-\frac{2J}{T} < l < 0. \quad (10)$$

Fig. 5. Variation of observer pole P_z with the coefficient l .Fig. 6. Simulation results of the discrete load torque observer with different l , where the gray dashed line represents the actual value of load torque, the black, red, blue solid lines represent the observed results with $l = l_0$, $l = 2l_0$, $l = 0.5l_0$, respectively.

Equation (10) means that, there is a limit of the convergence speed of discrete load torque observer. Define l_0 as the marginal value of l

$$l_0 = -\frac{2J}{T}. \quad (11)$$

Therefore, the maximum convergence speed of the discrete load torque observer is $e^{(l_0/J)t} = e^{(-2/T)t}$. Despite the observer is still stable if $l < l_0 < 0$, the observed load torque will be of a significant oscillation. Fig. 5 shows the relation between the discrete observer pole P_z and the coefficient l .

Fig. 6 shows the simulation results of the discrete load torque observer. The speed command steps from 0 to 1000 r/min at 0 s, the load torque steps from 0 to 2 N•m at 0.03 s, and the sampling frequency is 10⁴ Hz. The simulation results are the same as the theoretical analysis aforementioned, if $l = 2l_0$, the result of the discrete observer has a significant oscillation and rapid convergence. That means l_0 is the optimal value of l for the discrete-time load torque observer.

In industrial field, the load inertia is always 3–20 times the inertia of a servo motor. As the adjustable coefficient l depends only on the inertia J , it could be proper to let $l = (5–10)l_0$ with

the uncertain inertia. The load torque observer will converge to the actual value with any value of l below 0, but smaller l will lead to larger oscillation when motor speed changes. Hence, if the system inertia is unknown, it would be better to choose l as large as possible in order to ensure the stability and reliability of the control system.

Consequently, the observed value of the proposed load torque observer will be fed into the inertia identification algorithm as an input variable, and it can also be fed into the PI controller in the speed loop as a compensation of the load torque disturbance.

IV. INERTIA IDENTIFICATION ALGORITHM

A. FOREFOP

The traditional recursive empirical frequency-domain optimal parameter (REFOP) is a valid method for parameter identification, even if the system is subjected to colored noise. However, the original algorithm of REFOP is very complicated, and the most critical point is the order of intermediate variables of REFOP will become larger and larger along with the identification process. So the fixed-order REFOP algorithm is proposed in this section in order to reduce the complexity of the traditional REFOP algorithm. Furthermore, the FOREROP algorithm preserves the convergence and stability properties of the REFOP algorithm.

The equation of motion (1) can be rewritten in the frequency domain

$$\omega = \frac{1}{Js + B}(T_e - \tau_L). \quad (12)$$

Applying the Z transformation with zero-order hold, (12) leads

$$\begin{aligned} \omega(z) &= Z \left\{ \frac{1 - e^{-Ts}}{s} \frac{1}{Js + B} \right\} (T_e(z) - \tau_L(z)) \\ &= \frac{\frac{1}{B}(1 - e^{-\frac{B}{J}T})z^{-1}}{1 - e^{-\frac{B}{J}T} z^{-1}} (T_e(z) - \tau_L(z)) \\ &= \frac{b_1 z^{-1}}{1 + a_1 z^{-1}} (T_e(z) - \tau_L(z)). \end{aligned} \quad (13)$$

Based on (13), the estimated parameter θ and regressor $\varphi(k)$ are defined as follows:

$$\theta = [a_1, b_1]^T \quad (14)$$

$$\varphi(k) = [-\omega(k-1), (T_e(k-1) - \tau_L(k-1))]^T. \quad (15)$$

The estimation of θ at k th instant is expressed as

$$\begin{aligned} \hat{\theta}(k) &= \hat{\theta}(k-1) + d^{-1}(k)P(k-1) \\ &\quad \times [\Phi^T(k-1)\alpha(k) + c^{-1}(k)\sigma(k)\phi(k)] \\ &\quad \times [\omega(k) - \phi^T(k)\hat{\theta}(k-1)] \\ &\quad + d^{-1}(k)P(k-1) \\ &\quad \times [\phi(k) - c^{-1}(k)\phi^T(k)P(k-1)\phi(k)] \\ &\quad \times \Phi^T(k-1)\alpha(k)]\alpha^T(k) \\ &\quad \times [Y(k) - \Phi(k-1)\hat{\theta}(k-1)] \end{aligned} \quad (16)$$

$$\begin{aligned} P(k) &= P(k-1) - d^{-1}(k)P(k-1) \\ &\quad \times [\phi(k)\alpha^T(k)\Phi(k-1) + \Phi^T(k-1)\alpha(k)\phi^T(k)] \\ &\quad \times P(k-1) + c^{-1}(k)d^{-1}(k)P(k-1) \\ &\quad \times [\phi^T(k)P(k-1)\phi(k)\Phi^T(k-1)\alpha(k) \\ &\quad \times \alpha^T(k)\Phi(k-1) - \sigma(k)\phi(k)\phi^T(k)] \\ &\quad \times P(k-1). \end{aligned} \quad (17)$$

By defining the auxiliary signal

$$t(k) = T_e(k) - \tau_L(k) \quad (18)$$

$$t^*(k) = t^2(k) + t^2(k-1) + t^2(k-2). \quad (19)$$

All the intermediate variables in (16) and (17) are expressed as follows:

$$\Phi(k) = [\phi(k-1), \phi(k)]^T \quad (20)$$

$$Y(k) = [\omega(k-1), \omega(k)]^T \quad (21)$$

$$\begin{aligned} \alpha(k) &= [1, 1]^T \times (t(k)t(k-1) \\ &\quad + t(k-1)t(k-2) + t(k)t(k-2)) \end{aligned} \quad (22)$$

$$\begin{aligned} \sigma(k) &= t^*(k) - \alpha^T(k)\Phi(k-1)P(k-1) \\ &\quad \times \Phi^T(k-1)\alpha(k) \end{aligned} \quad (23)$$

$$c(k) = 1 + \phi^T(k)P(k-1)\Phi^T(k-1)\alpha(k) \quad (24)$$

$$d(k) = c(k) + c^{-1}(k)\sigma(k)\phi^T(k)P(k-1)\phi(k). \quad (25)$$

All of the initial value in (18)–(25) can be set as 0, and the initial value of $P(k)$ can be set as a unit matrix for the sake of simplicity.

Then, the estimated inertia of PMSM can be got by solving the following equation:

$$\begin{cases} \hat{B} = \frac{1 + a_1}{b_1} \\ \hat{J} = -\frac{\hat{B}T}{\ln(-a_1)} \end{cases}. \quad (26)$$

The standard REFOP algorithm also uses (16) and (17) as the recursive equations, but the intermediate variables in (20)–(25) are different from the proposed FOREFOP. The intermediate variables of standard REFOP are shown as follows:

$$\Phi'(k) = [j(1), j(2), \dots, j(k)]^T \quad (27)$$

$$Y'(k) = [\omega(1), \omega(2), \dots, \omega(k)]^T \quad (28)$$

$$\begin{aligned} \alpha'(k) &= \sum_{i=1}^k t(k)(t_e(i-1, k), t_e(i-2, k), \dots, \\ &\quad t_e(i-k+1, k)) \end{aligned} \quad (29)$$

$$\begin{aligned} \sigma'(k) &= \left(\sum_{i=1}^k t^2(i) \right) - \alpha^T(k)\Phi(k-1)P(k-1) \\ &\quad \times \Phi^T(k-1)\alpha(k) \end{aligned} \quad (30)$$

$$c'(k) = 1 + \phi^T(k)P(k-1)\Phi^T(k-1)\alpha(k) \quad (31)$$

$$d'(k) = c(k) + c^{-1}(k)\sigma(k)\phi^T(k)P(k-1)\phi(k) \quad (32)$$

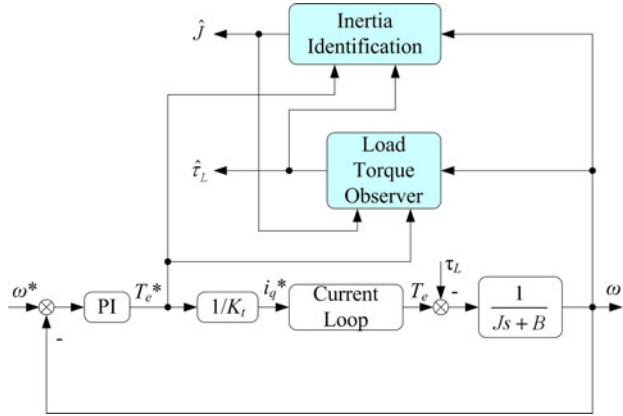


Fig. 7. Control diagram of the inertia identification algorithm with the load torque observer.

where

$$t_e(i, m) = \begin{cases} t(i) & 1 \leq i \leq m \\ t(i + m) & 1 - m \leq i \leq 0 \end{cases}. \quad (33)$$

It can be seen that the orders of matrices become larger with the increase of recursive times; therefore, the standard REFOP algorithm is not suitable for a real-time control system, such as a DSP based servo system. In comparison, the proposed FOREFOP algorithm can fix the orders of matrices to meet the need of real-time control for the servo system. The modification of FOREFOP is fixing the sampling points to two, which means the proposed algorithm is part of standard REFOP. As proved in [25] that, because the input signals (i.e., the variables t and t^*) are stressed in (18) and (19), the proposed inertia identification algorithm is robust against noise interference. Hence, the FOREFOP retains the convergence and robustness of standard REFOP, which can also be proved by the following simulation and experiment.

Moreover, the load torque τ_L in (15) can be replaced by the observed value $\hat{\tau}_L$ in the proposed load torque observer. And the motor parameter J in the load torque observer can also be substituted by the estimated value \hat{J} , as the proposed FOREFOP algorithm has a certain robustness against colored noise. Due to the fact that the effect of friction coefficient B is much smaller than the inertia J , B is treated as its initial value in this paper for the simplicity of analysis and application. The control diagram of the proposed FOREFOP algorithm with load torque observer is shown in Fig. 7.

B. Simulation Comparison With RLS

In this section, the simulation waveforms of the proposed FOREFOP algorithm are shown, and the simulation results of RLS are also shown as a comparison. The RLS algorithm is an effective method for parameter identification in the industrial field. However, there is only one adjustable parameter in the RLS algorithm, i.e., the forgetting factor. The value range of forgetting factor is 0–1, and it is usually chosen between 0.95 and 0.99 for the convergence and stability of the identification algorithm. In this paper, the forgetting factor of the RLS

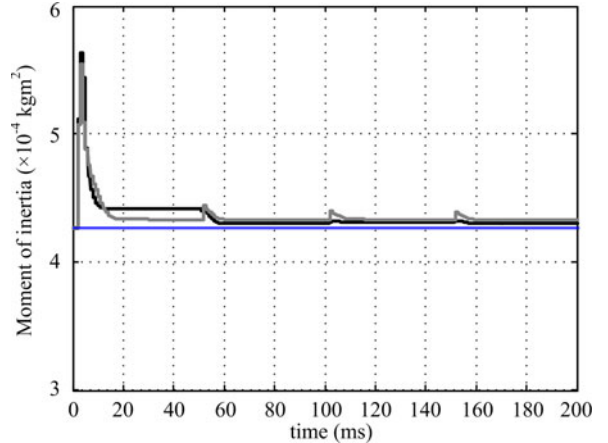


Fig. 8. Simulation comparison of FOREFOP and RLS with load torque observers, and the load torque is 0. Where the bold black line is the estimated inertia of FOREFOP, the bold gray line is the estimated inertia of RLS, and the blue line is the actual inertia.

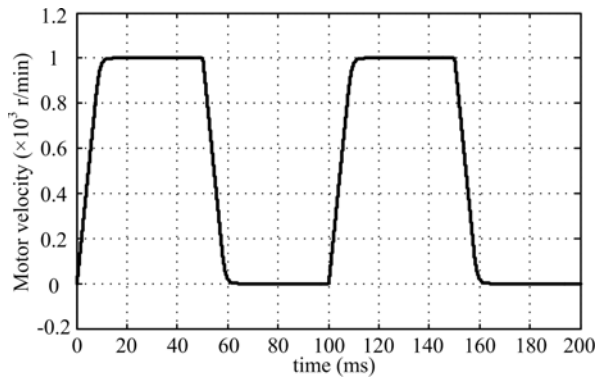


Fig. 9. Simulated speed velocity of PMSM with 0 load torque.

algorithm is set as 0.99 in both of the simulation and experiment. Both of the simulation conditions of FOREFOP and RLS are identical.

Fig. 8 exhibits the inertia identification results without load torque. The speed response is shown in Fig. 9. It can be seen from Fig. 8 that the estimated inertia value of inertia using FOREFOP in steady state is closer to the actual value than that of RLS. The estimated errors in steady state of FOREFOP and RLS are 1.0% and 1.5%, respectively. The identified results are with fluctuation at speed step, it can be explained by system delays. Both of the current response and speed response lag their relevant commands because the servo system can be treated as a low-pass inertial system. The current control frequency (10 kHz) is ten times the speed control frequency (1 kHz), therefore, the speed response lags behind the current response, and the delays may deteriorate the identified results especially in speed dynamic. In speed dynamic process, the fluctuation of the estimated inertia value of RLS is larger than that of FOREFOP, which means the FOREFOP algorithm is of better robustness than the RLS algorithm against the system delays. However, the estimated result of FOREFOP converges to the true value more slowly than that of RLS. This is because the establishing process of intermediate variables of FOREFOP is more complex than

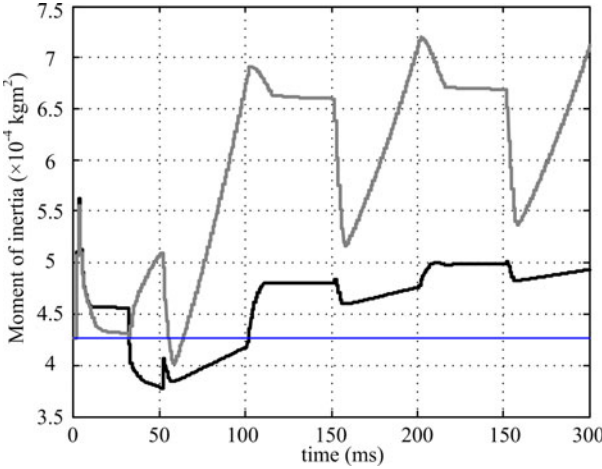


Fig. 10. Simulation comparison of FOREFOP and RLS without load torque observer at 2-N•m load torque, where the bold black line is the estimated inertia of FOREFOP, the bold gray line is the estimated inertia of RLS, and the blue line is the actual inertia.

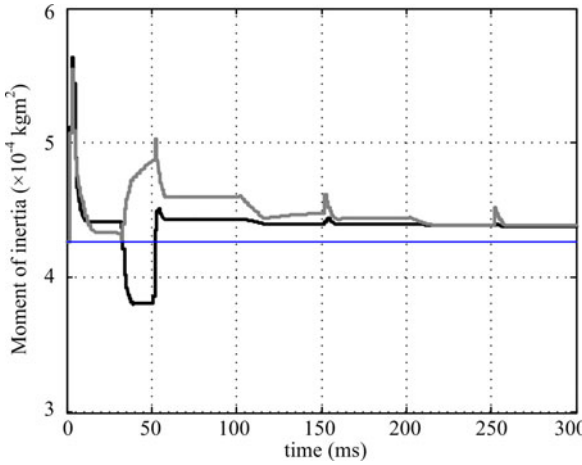


Fig. 11. Simulation comparison of FOREFOP and RLS with load torque observer at 2-N•m load torque, where the bold black line is the estimated inertia of FOREFOP, the bold gray line is the estimated inertia of RLS, and the blue line is the actual inertia.

RLS, i.e., FOREFOP needs two steps previous values but RLS needs only one step previous values.

Figs. 10 and 11 exhibit the inertia identification results with 2-N•m load torque. Where the bold black lines are the estimated inertia of FOREFOP, the bold gray lines are the estimated inertia of RLS, and the blue lines are the actual inertia of PMSM. The speed response in both figures is shown in Fig. 12 and the load torque steps from 0 to 2 N•m at 0.03 s.

Fig. 10 shows that the estimated result of RLS has a large bias against the actual inertia. On the contrary, the estimated result of FOREFOP is still around the actual inertia within the error of 17.2%. That means the FOREFOP algorithm has a strong robustness against colored noise. With the load torque observer in Fig. 11, the estimated results of both the algorithms are the same as which in Fig. 8, and the estimated errors of FOREFOP and RLS in steady state are 2.7% and 3.1%, respectively.

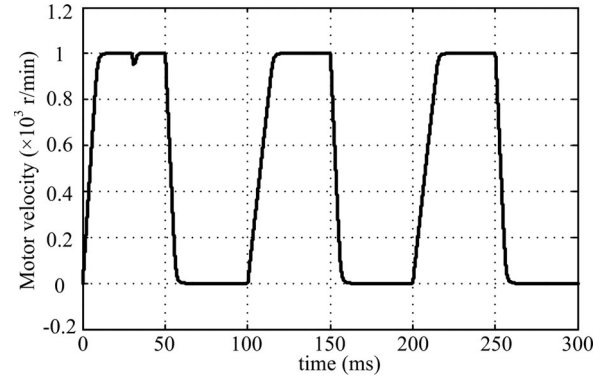


Fig. 12. Simulated speed velocity of PMSM with 2-N•m load torque.

V. STRUCTURE OF SPEED LOOP

The speed diagram is shown as Fig. 2. Assuming the simplified close-loop transfer function of current loop $G_{cc}(s)$ is (34), the open-loop transfer function of speed loop $G_{so}(s)$ is expressed in (35)

$$G_{cc}(s) = \frac{K_t}{T_{cc}s + 1}. \quad (34)$$

where T_{cc} is the time constant of the current loop

$$G_{so}(s) = \left(K_P + \frac{K_I}{s} \right) \frac{1}{(T_{cc}s + 1)(Js + B)}. \quad (35)$$

With the definition of cutoff frequency and phase margin of open loop, (36) and (37) are obtained

$$|G_{so}(j\omega_{sc})| = \frac{\sqrt{K_P^2 + \frac{K_I^2}{\omega_{sc}^2}}}{\sqrt{T_{cc}^2 \omega_{sc}^2 + 1} \sqrt{J^2 \omega_{sc}^2 + B^2}} = 1 \quad (36)$$

$$\begin{aligned} \angle G_{so}(j\omega_{sc}) &= -\arctan \frac{K_I}{\omega_{sc} K_P} - \arctan(\omega_{sc} T_{cc}) \\ &\quad - \arctan \frac{J\omega_{sc}}{B} = \varphi_m - p. \end{aligned} \quad (37)$$

where ω_{sc} is the cutoff frequency of the speed loop, and φ_m is the phase margin of the speed loop.

The expression of K_P (38) and K_I (39) can be obtained by solving (36) and (37)

$$\begin{aligned} K_P &= \sqrt{(1 + T_{cc}^2 \omega_{sc}^2)(J^2 \omega_{sc}^2 + B^2)} \\ &\times \sin \left(\varphi_m - \arctan \left(\frac{1}{\omega_{sc} T_{cc}} \right) + \arctan \frac{J\omega_{sc}}{B} \right) \end{aligned} \quad (38)$$

$$\begin{aligned} K_I &= \omega_{sc} \sqrt{(1 + T_{cc}^2 \omega_{sc}^2)(J^2 \omega_{sc}^2 + B^2)} \\ &\times \cos \left(\varphi_m - \arctan \left(\frac{1}{\omega_{sc} T_{cc}} \right) + \arctan \frac{J\omega_{sc}}{B} \right) \end{aligned} \quad (39)$$

In order to simplify the calculation process, we make the following assumption that, $T_{cc}\omega_{sc} \ll l_1$ and $J\omega_{sc} \gg B$. As in general, the current loop bandwidth ($1/T_{cc}$) is much larger than the speed loop bandwidth (ω_{sc}), and the friction coefficient B is much smaller than the production of $J\omega_{sc}$. Consequently, the limitation of speed loop bandwidth is $1/T_{cc} \gg \omega_{sc} \gg B/J$. At

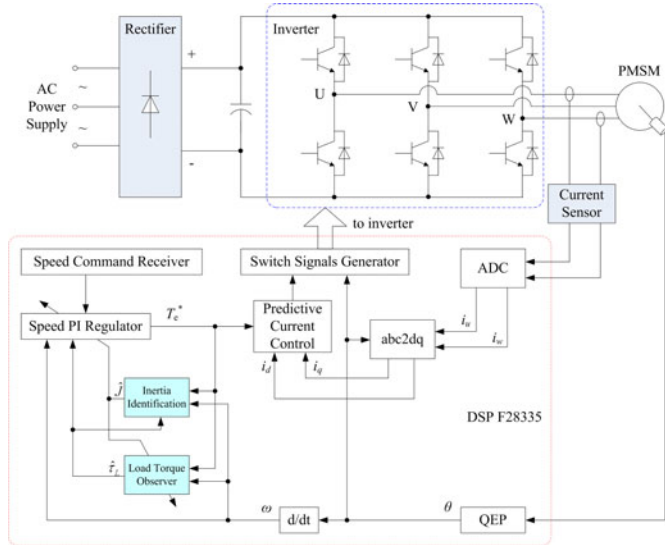


Fig. 13. Overall control structure of the proposed algorithm.

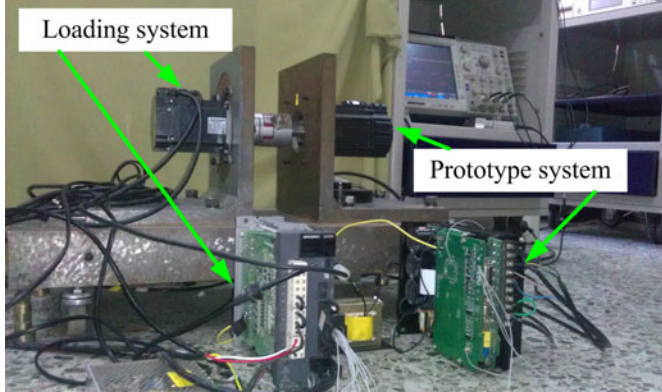


Fig. 14. Photograph of the experiment platform.

last, the simplified calculation process of K_P (38) and K_I (39) are shown as (40) and (41), respectively

$$K_P = J\omega_{sc} \sin \varphi_m \quad (40)$$

$$K_I = J\omega_{sc}^2 \cos \varphi_m. \quad (41)$$

VI. EXPERIMENTS

A. Experimental Setup

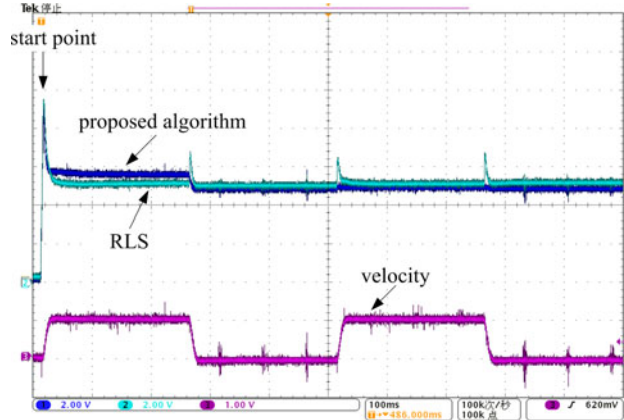
In order to verify the proposed algorithm, an experiment system as shown in Fig. 13 is set up. Fig. 13 shows the overall control structure with the proposed on-line inertia identification algorithm and the load torque observer. And the photograph of the experiment platform is shown in Fig. 14. Where a Mitsubishi J-3 servo pack is coupled with the prototype motor for the loading test.

Table I summarizes the specifications of the PMSM used in this paper, and the precision of the encoder is 2500 ppr. And the switch frequency of the inverter in this paper is 10 kHz.

It has been proved that, the optimal bandwidth of the current loop is one twelfth of the switching frequency, i.e., 833 Hz

TABLE I
PMSM SPECIFICATIONS

Symbol	Quantity
Rated Power	750 W
Rated Torque	2.39 N·m
Rated Speed	3000 r/min
Rated Current	4.8 A
Number of pole-pairs	4
Inductance L_{dq}	3.9 mH
Resistance R	0.45 Ω
Moment of inertia J (with loading motor)	$4.27 \times 10^{-4} \text{ kg}\cdot\text{m}^2$

Fig. 15. Experimental comparison between the FOREFOP and RLS with no load, and repeated speed command. Where the identified of inertia is $2 \times 10^{-4} \text{ kg}\cdot\text{m}^2/\text{div}$ and the speed is 1000 r/min/div.

in this paper. Then, the cutoff frequency of speed loop can be chosen as $\omega_{sc} = 150$ Hz, and the PI parameters of a discrete control system, which are calculated from (33) and (34), are $K_p = 0.767$ and $K_i = 0.334$. In order to decrease the overshoot of the speed response, an antiwindup algorithm proposed in [32] is also adopted.

B. Experiment Results

In this section, all of the observed variables are obtained with the DAC module embedded within the DSP, and collected by an oscilloscope.

Fig. 15 gives the experimental comparison between the proposed FOREFOP algorithm and RLS algorithm without load, where the speed command is 1000–0 r/min repeated. It is similar to the simulation comparison in Fig. 8, the FOREFOP algorithm converges to the actual inertia value a little slower than the RLS algorithm, and the fluctuation of the FOREFOP in steady state is much smaller than the RLS. In the real system, both of the quantization noise and sampling filtering will also influence the identified results. The identified errors of the FOREFOP and RLS algorithms are 12.5% and 17.2%, respectively. The identification error is much larger than the simulation result, it is not only because the current and speed sensors are not as precise as in simulation result, it is not only because the current and speed sensors are not as precise as in simulation, but also because the system noise in the actual system.

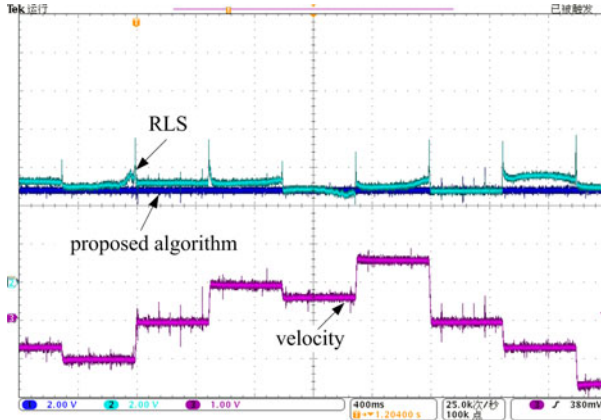


Fig. 16. Experimental comparison between the FOREFOP and RLS without load, and random step speed command. Where the identified of inertia is $2 \times 10^{-4} \text{ kg}\cdot\text{m}^2/\text{div}$ and the speed is 1000 r/min/div.

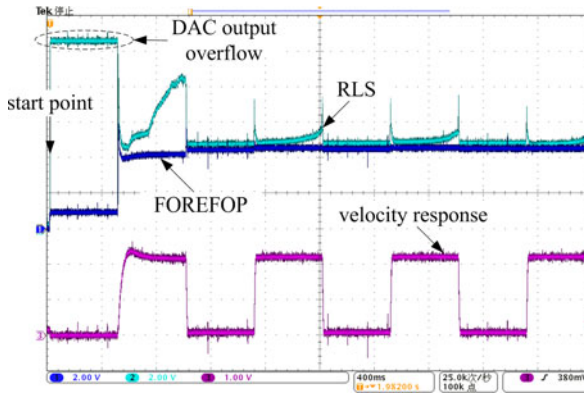


Fig. 17. System responses with initial value $\hat{J} = J/5$ under 0 load torque condition. Where the identified inertia is $2 \times 10^{-4} \text{ kg}\cdot\text{m}^2/\text{div}$ and the speed is 500 r/min/div.

Fig. 16. shows the experimental comparison between the proposed FOREFOP algorithm and RLS algorithm without load, and the speed command are random steps. It can be found that, the identified result of RLS has a spike at every instant when the speed changes, on the contrary, the identified result of FOREFOP are still stable whether the speed changes or not.

Figs. 17 and 18 exhibit the responses of the proposed control system with the initial value of $\hat{J} = j/5$ and $\hat{J} = 5j$, respectively. The speed command is 1000–0 r/min repeated, and the load torque is 0. It can be seen that, the results of FOREFOP will converge to the actual value within three or four speed changes, and the identified inertia can be used to modify the PI regulator in order to obtain the optimal speed responses. On the contrary, the results of RLS exceed the output limitation of DAC at the beginning. The reason is that the speed command and feedback are both 0 r/min at the start moment, but the feedback current is not exactly zero due to the error of ADC and all the intermediate variables are not established correctly. Therefore, the color noise leads to a larger identification error at the beginning. It also proves the proposed FOREFOP algorithm has stronger capability of noise immunity than the RLS.

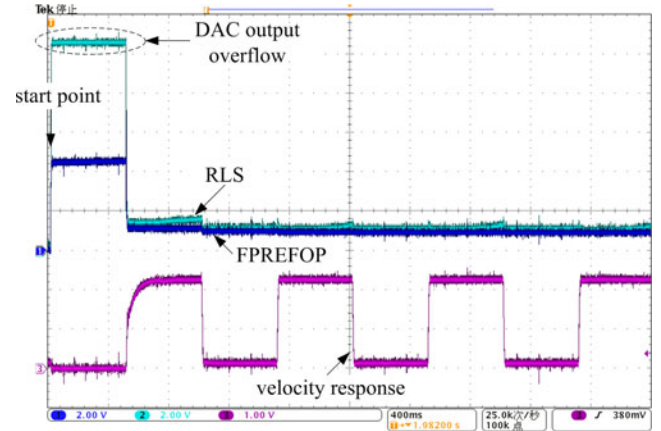


Fig. 18. System responses with initial value $\hat{J} = 5J$ under 0 load torque condition. Where the identified inertia is $1 \times 10^{-3} \text{ kg}\cdot\text{m}^2/\text{div}$, and the speed is 500 r/min/div.

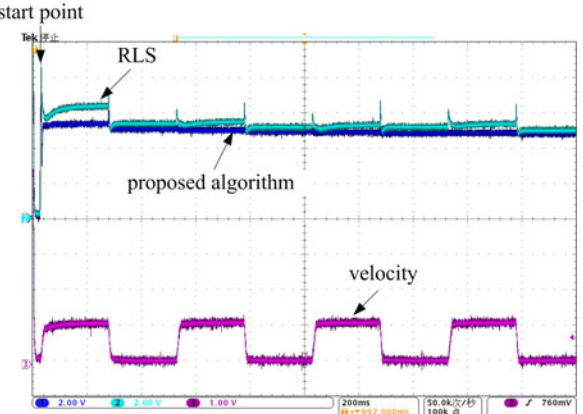


Fig. 19. Experimental comparison of the FOREFOP and RLS with 2-N•m load, and repeated speed command. Where the estimated inertia is $2 \times 10^{-4} \text{ kg}\cdot\text{m}^2/\text{div}$ and the speed is 1000 r/min/div.

Fig. 19 shows the estimated inertia of FOREFOP and RLS with 2-N•m load torque, and Fig. 20 shows the output of the load torque observer when the speed command is 1000–0 r/min repeated. In Fig. 19, it can be seen that the estimated inertia of RLS has a little deviation from the actual value due to the disturbance of the loading system and the delay of the load torque observer. When the speed changes two times, the estimated inertia of RLS converges to the actual value precisely. However, the proposed FOREFOP algorithm still exhibits the robustness against the disturbance of load torque and other noise, and the estimated inertia of FOREFOP is more close to the actual value. The estimated errors of FOREFOP and RLS are 12.5% and 21.9%, respectively. In Fig. 20, the observed load torque has a little oscillation at every speed change as the result of sampling delay and sampling precision of the motor speed and phase current. In order to simulate the condition of resistive load, the loading servo pack (Mitsubishi J-3 servo pack) is set to work in the speed control mode (speed command is 0 r/min) and the torque limitation is set as the required load torque (2 N•m). As shown in Fig. 20, the speed error of the loading servo pack is negative (-1000 r/min) due to the speed of driving motor is

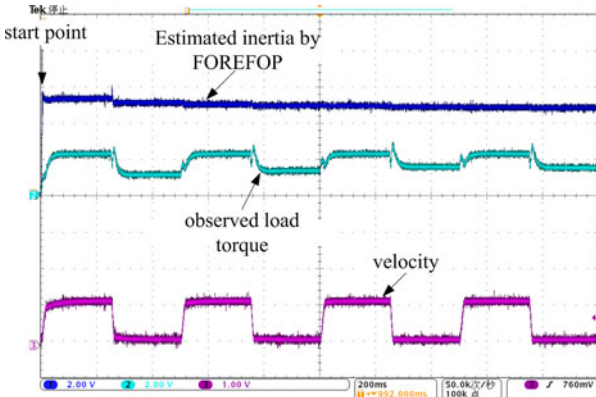


Fig. 20. Experimental results of load torque observer and proposed FOREFOP inertia identification algorithm. Where the estimated inertia is $2 \times 10^{-4} \text{ kg}\cdot\text{m}^2/\text{div}$, the observed load torque is $2 \text{ N}\cdot\text{m}/\text{div}$ and the speed is $1000 \text{ r/min}/\text{div}$.

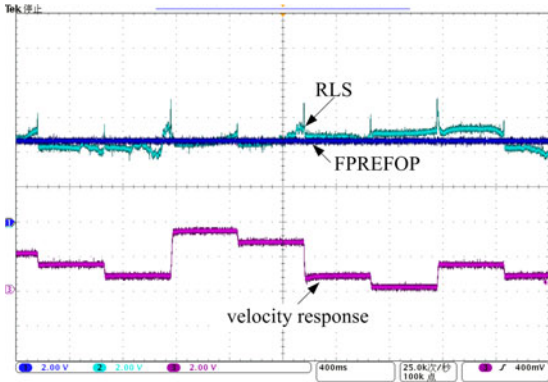


Fig. 21. Experimental comparison of the FOREFOP and RLS with $2 \text{ N}\cdot\text{m}$ load torque, and random step speed command. Where the estimated inertia is $2 \times 10^{-4} \text{ kg}\cdot\text{m}^2/\text{div}$ and the speed is $1000 \text{ r/min}/\text{div}$.

positive (1000 r/min), hence, the loading servo pack needs a positive speed error to decrease the accumulation of the Integrator. It means if there is no reverse speed (i.e., there is no positive speed error) for the loading servo pack, the accumulation of the Integrator will be kept as a nonzero constant at zero speed, consequently, the load torque during zero speed is $0\text{--}2 \text{ N}\cdot\text{m}$. But the nonzero loading condition has little impact on estimated inertia, which can be proved by the experiment waveforms in Figs. 19 and 20.

Fig. 21 exhibits the experimental results of RLS and proposed FOREFOP algorithms with $2 \text{ N}\cdot\text{m}$ load torque, with speed command of random steps. Similarly to Fig. 16, the identified result of RLS has a spike at every speed change, and the identification error is larger at the lower speed. On the other hand, the FOREFOP algorithm cannot only calculate the inertia from the limited information, but also resist the system noise and other errors.

Corresponding to Figs. 17 and 18, Figs. 22 and 23 exhibit the responses of the proposed control system with the initial value of $\hat{J} = J/5$ and $\hat{J} = 5J$, respectively. The difference is the load torque is $2 \text{ N}\cdot\text{m}$. And the speed command is $1000\text{--}0 \text{ r/min}$ repeated. These figures show that, the estimated inertia of the proposed FOREFOP algorithm can converge to the actual

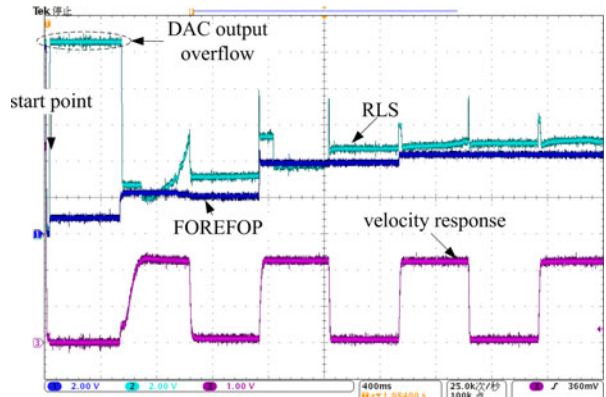


Fig. 22. System responses with initial value $\hat{J} = J/5$, and $2 \text{ N}\cdot\text{m}$ load torque. Where the identified inertia is $2 \times 10^{-4} \text{ kg}\cdot\text{m}^2/\text{div}$ and the speed is $500 \text{ r/min}/\text{div}$.

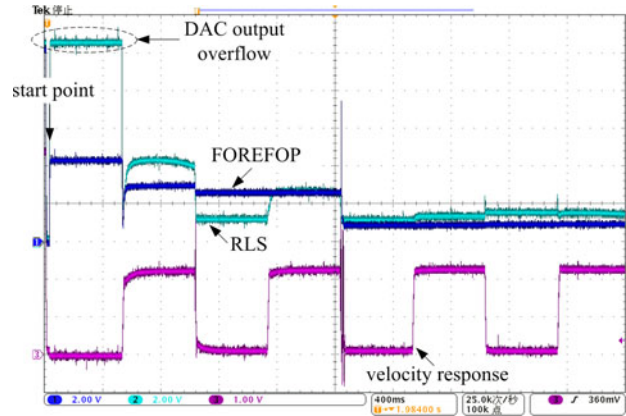


Fig. 23. System responses with initial value $\hat{J} = 5J$, and $2 \text{ N}\cdot\text{m}$ load torque. Where the identified inertia is $1 \times 10^{-3} \text{ kg}\cdot\text{m}^2/\text{div}$ and the speed is $500 \text{ r/min}/\text{div}$.

value fast and precisely, no matter what the initial value and the loading condition.

VII. CONCLUSION

In order to identify the moment of inertia on-line, a novel inertia identification algorithm with load torque observer is proposed in this paper, which is named FOREFOP. The proposed FOREFOP algorithm is more suitable for industrial real-time control system and can resist the disturbance of system delay and other errors. The load torque observer is based on Gopinath's theory, and the characteristics of the load torque observer are simple structure, easy realization, and precise result. With the estimated inertia and load torque, a calculation method for the speed loop PI parameters in frequency domain is proposed, and the relationship of PI parameters and speed loop bandwidth is also presented.

Both of the simulation and experimental results show the proposed FOREFOP algorithm, compared with RLS algorithm, is more precise and robust against load torque disturbance and the error of system sampling and filtering.

ACKNOWLEDGMENT

The authors would like to thank the anonymous reviewers and the editors for their helpful comments on an earlier draft of this paper.

REFERENCES

- [1] M. Mengoni, L. Zarri, A. Tani, G. Erra, and D. Casadei, "A comparison of four robust control schemes for field-weakening operation of induction motors," *IEEE Trans. Power Electron.*, vol. 27, no. 1, pp. 307–320, Jan. 2012.
- [2] S. Ziaeinejad, Y. Sangsefidi, H. P. Nabi, and A. Shoulaie, "Direct torque control of two-phase induction and synchronous motors," *IEEE Trans. Power Electron.*, vol. 28, no. 8, pp. 4041–4050, Aug. 2013.
- [3] F. J. Lin, J. C. Hwang, P. H. Chou, and Y. C. Hung, "FPGA-based intelligent-complementary sliding-mode control for PMLSM servo-drive system," *IEEE Trans. Power Electron.*, vol. 25, no. 10, pp. 2573–2587, Oct. 2010.
- [4] D. Li-Jun, S. Da-nan, D. Kan, Z. Lei-Ting, and L. Zhi-Gang, "Optimized design of discrete traction induction motor model at low-switching frequency," *IEEE Trans. Power Electron.*, vol. 28, no. 10, pp. 4803–4810, Oct. 2013.
- [5] A. M. Bazzi, A. Dominguez-Garcia, and P. T. Krein, "Markov reliability modeling for induction motor drives under field-oriented control," *IEEE Trans. Power Electron.*, vol. 27, no. 2, pp. 534–546, Feb. 2012.
- [6] M. Masiola, B. Vafakhah, J. Salmon, and A. M. Knight, "Fuzzy self-tuning speed control of an indirect field-oriented control induction motor drive," *IEEE Trans. Ind. Appl.*, vol. 44, no. 6, pp. 1732–1740, Nov./Dec. 2008.
- [7] O. Wallmark, S. Lundberg, and M. Bongiorno, "Input admittance expressions for field-oriented controlled salient PMSM drives," *IEEE Trans. Neural Netw.*, vol. 27, no. 3, pp. 1514–1520, Mar. 2012.
- [8] M. Pacas and J. Weber, "Predictive direct torque control for the PM synchronous machine," *IEEE Trans. Ind. Electron.*, vol. 52, no. 5, pp. 1350–1356, Oct. 2005.
- [9] S. K. Sahoo, S. Dasgupta, S. K. Panda, and J. X. Xu, "A lyapunov function-based robust direct torque controller for a switched reluctance motor drive system," *IEEE Trans. Power Electron.*, vol. 27, no. 2, pp. 555–564, Feb. 2012.
- [10] A. Bouafia, J.-P. Gaubert, and F. Krim, "Predictive direct power control of three-phase pulsewidth modulation (PWM) rectifier using space-vector modulation (SVM)," *IEEE Trans. Power Electron.*, vol. 25, no. 1, pp. 228–236, Jan. 2010.
- [11] H. Jiabing and Z. Q. Zhu, "Improved voltage-vector sequences on dead-beat predictive direct power control of reversible three-phase grid-connected voltage-source converters," *IEEE Trans. Power Electron.*, vol. 28, no. 1, pp. 254–267, Jan. 2013.
- [12] M. Oettmeier, C. Heising, V. Staudt, and A. Steimel, "Dead-beat control algorithm for single-phase 50-kW AC railway grid representation," *IEEE Trans. Power Electron.*, vol. 25, no. 5, pp. 1184–1192, May 2010.
- [13] L. Niu, M. Yang, and D. G. Xu, "An adaptive robust predictive current control for PMSM with online inductance identification," *Int. Rev. Electr. Eng.*, vol. 7, no. 2, pp. 3845–3856, Mar./Apr. 2012.
- [14] S. A. Davari, D. A. Khaburi, F. Wang, and R. M. Kennel, "Using full order and reduced order observers for robust sensorless predictive torque control of induction motors," *IEEE Trans. Power Electron.*, vol. 27, no. 7, pp. 3424–3433, Jul. 2012.
- [15] J. C. Moreno, J. M. E. Huerta, R. G. Gil, and S. A. Gonzalez, "A robust predictive current control for three-phase grid-connected inverters," *IEEE Trans. Ind. Electron.*, vol. 56, no. 6, pp. 1993–2004, Jun. 2009.
- [16] J. M. E. Huerta, J. C. Moreno, J. R. Fischer, and R. G. Gil, "A synchronous reference frame robust predictive current control for three-phase grid-connected inverters," *IEEE Trans. Ind. Electron.*, vol. 57, no. 3, pp. 954–962, Mar. 2010.
- [17] K. B. Lee, J. Y. Yoo, J. H. Song, and I. Choy, "Improvement of low speed operation of electric machine with an inertia identification using ROELO," *IEE Proc.—Electr. Power Appl.*, vol. 151, no. 1, pp. 116–120, Jan. 2004.
- [18] J. W. Choi, S. C. Lee, and H. G. Kim, "Inertia identification algorithm for high-performance speed control of electric motors," *IEE Proc.—Electr. Power Appl.*, vol. 153, no. 3, pp. 379–386, May 2006.
- [19] W. S. Huang, C. W. Liu, P. L. Hsu, and S. S. Yeh, "Precision control and compensation of servomotors and machine tools via the disturbance observer," *IEEE Trans. Ind. Electron.*, vol. 57, no. 1, pp. 420–429, Jan. 2010.
- [20] T. J. Kweon and D. S. Hyun, "High-performance speed control of electric machine using low-precision shaft encoder," *IEEE Trans. Power Electron.*, vol. 14, no. 5, pp. 838–849, Sep. 1999.
- [21] F. J. Lin, "Robust speed-controlled induction-motor drive using EKF and RLS estimators," *IEE Proc.—Electr. Power Appl.*, vol. 143, no. 3, pp. 186–192, May 1996.
- [22] Y. Okamura, Y. Chun, and Y. Hori, "Inertia moment identification in the average speed-type instantaneous speed observer," *Elect. Eng. Japan*, vol. 115, no. 7, pp. 120–129, Dec. 1995.
- [23] F. Andoh, "Inertia identification method based on the product of the integral of torque reference input and motor speed," in *Proc. IEEE Int. Conf. Control Appl.*, San Antonio, TX, USA, 2008, pp. 1151–1158.
- [24] F. Andoh, "Moment of inertia identification using the time average of the product of torque reference input and motor position," *IEEE Trans. Power Electron.*, vol. 22, no. 6, pp. 2534–2542, Nov. 2007.
- [25] K. Lo, H. Kimura, W. H. Kwon, and X. J. Yang, "Empirical frequency-domain optimal parameter estimate for black-box processes," *IEEE Trans. Circuits Syst. I, Reg. Papers*, vol. 53, no. 2, pp. 419–430, Feb. 2006.
- [26] K. Lo, H. Kimura, and W. H. Kwon, "New identification approaches for disturbed models," *Automatica*, vol. 39, no. 9, pp. 1627–1634, Sep. 2003.
- [27] B. Gopinath, "On the control of linear multiple input-output systems," *Bell Syst. Tech. J.*, vol. 50, no. 3, pp. 1063–1081, 1971.
- [28] K. Natori, T. Tsuji, K. Ohnishi, A. Hace, and K. Jezernik, "Time-delay compensation by communication disturbance observer for bilateral tele-operation under time-varying delay," *IEEE Trans. Ind. Electron.*, vol. 57, no. 3, pp. 1050–1062, Mar. 2010.
- [29] H. Kobayashi, S. Katsura, and K. Ohnishi, "An analysis of parameter variations of disturbance observer for motion control," *IEEE Trans. Ind. Electron.*, vol. 54, no. 6, pp. 3413–3421, Dec. 2007.
- [30] D. Zhang, H. Li, and E. G. Collins, "Digital anti-windup PI controllers for variable-speed motor drives using FPGA and stochastic theory," *IEEE Trans. Power Electron.*, vol. 21, no. 5, pp. 1496–1501, Sep. 2006.
- [31] C. C. Chan, J. Z. Jiang, W. Xia, and K. T. Chan, "Novel wide range speed control of permanent magnet brushless motor drives," *IEEE Trans. Power Electron.*, vol. 10, no. 5, pp. 539–546, Sep. 1995.
- [32] H. B. Shin and J. G. Park, "Anti-windup PID controller with integral state predictor for variable-speed motor drives," *IEEE Trans. Ind. Electron.*, vol. 59, no. 3, pp. 1509–1516, Mar. 2012.



Li Niu was born in Heilongjiang, China, in 1985. He received the B.S. and M.S. degrees in electrical engineering from the Harbin Institute of Technology, Harbin, China, in 2008 and 2010, respectively, where he is currently working toward the Ph.D. degree.

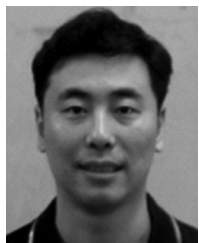
His research interests include power electronics, and servo drive of PMSM.



Dianguo Xu (M'97–SM'12) was born in Heilongjiang Province, China, in 1960. He received the B.S. degree in control engineering from the Harbin Shipbuilding Engineering Institute, Harbin, China, in 1981, and the M.S. and Ph.D. degrees in electrical engineering from the Harbin Institute of Technology, Harbin, in 1984 and 1990, respectively.

Since 1994, he has been a Professor with the Department of Electrical Engineering, Harbin Institute of Technology. He was the Department Head from 1992 to 1998, the Dean of School of Electrical Engineering and Automation from 1998 to 2010, and an Assistant President of the Harbin Institute of Technology from 2010 to present. His current research interests include ac motor drives, utility applications of power electronics, motion control, appliance intelligent control, lighting electronics, and robot control system.

Dr. Xu is the Chairman of the IEEE Harbin section and a member of the China Electrotechnical Society, China Automation Association, and China Power Supply Society. He has been a member of the International Steering Committee, IEEE International Conference on Power Electronics and Drive Systems; Technical Program Committee, International Conference on Electrical Machines and Systems; and Technical Program Committee, International Power Electronics and Motion Control Conference. He is the Technical Program Chair of the 2008 IEEE Vehicle Power and Propulsion Conference.



Ming Yang was born in Heilongjiang, China, in 1978. He received the B.S., M.S., and Ph.D. degrees in electrical engineering from the Harbin Institute of Technology, Harbin, China, in 2001, 2003, and 2007, respectively.

Since 2008 he has been an Assistant Professor with the Department of Electrical Engineering, Harbin Institute of Technology. His research interests include power electronics, servo drive of PMSM, automatic control, and intelligent control.



Zijian Liu was born in Heilongjiang, China, in 1989. He received the B.S. degree in electrical engineering from the Huazhong University of Science and Technology, Wuhan, China, in 2012, and is working toward the M.S. degree in electrical engineering from the Harbin Institute of Technology, Harbin, China.

His current research interests include the controller-autotuning in servo drives of PMSM.



Xianguo Gui was born in Inner Mongolia, China, in 1972. He received the B.S., M.S., and Ph.D. degrees in electrical engineering from the Harbin Institute of Technology, Harbin, China, in 1994, 1996, and 2000, respectively.

Since 2009 he has been an Associate Professor with the Department of Electrical Engineering, Harbin Institute of Technology. His research interests include ac drives, magnetic integration, and multiphysics analysis of electrical machines.